The Cape Mendocino, California, Earthquakes of April 1992: Subduction at the Triple Junction

D. Oppenheimer, G. Beroza, G. Carver, L. Dengler, J. Eaton, L. Gee, F. Gonzalez, A. Jayko, W. H. Li, M. Lisowski, M. Magee, G. Marshall, M. Murray, R. McPherson, B. Romanowicz, K. Satake, R. Simpson, P. Somerville, R. Stein, D. Valentine

The 25 April 1992 magnitude 7.1 Cape Mendocino thrust earthquake demonstrated that the North America–Gorda plate boundary is seismogenic and illustrated hazards that could result from much larger earthquakes forecast for the Cascadia region. The shock occurred just north of the Mendocino Triple Junction and caused strong ground motion and moderate damage in the immediate area. Rupture initiated onshore at a depth of 10.5 kilometers and propagated up-dip and seaward. Slip on steep faults in the Gorda plate generated two magnitude 6.6 aftershocks on 26 April. The main shock did not produce surface rupture on land but caused coastal uplift and a tsunami. The emerging picture of seismicity and faulting at the triple junction suggests that the region is likely to continue experiencing significant seismicity.

On 25 April 1992 at 18:06 (UTC), a surface wave magnitude (M_s) 7.1 earthquake occurred near the town of Petrolia, California (Fig. 1). The main shock was followed the next day by two M_s 6.6 aftershocks at 07:41 and 11:41, located offshore about 25 km west-northwest of Petrolia. These three earthquakes and more than 2000 recorded aftershocks illuminated the configuration of the Mendocino Triple Junction, where the Pacific, North America, and southernmost Juan de Fuca (Gorda) plates meet. The occurrence of a M 7 earthquake is not unusual at the triple junction; over 60 earthquakes of Modified Mercalli intensity ≥ VI (*1*) or M ≥ 5.5 have occurred there since 1853 (*2*). However, this earthquake sequence may have provided the first direct evidence of interplate seismicity and thus impacts regional hazard assessment. In this article, we describe geophysical and seismological observations and discuss implications for seismic hazards in the Pacific Northwest.

Damage estimates ranged from $48 million to $66 million and President Bush declared the region a major disaster area. Much of the damage resulted from the main shock; however, fires triggered by the first large aftershock destroyed most of the Scotia shopping district, and both large, off-shore aftershocks caused additional structural damage. The relatively low incidence of injuries and structural damage caused by this sequence is primarily the result of low population density and the predominance of small, wood frame structures in the epicentral area. The sequence caused 356 reported injuries, destroyed 202 buildings, and caused damage to an additional 906 structures primarily in the towns of Petrolia, Ferndale, Rio Dell, Scotia, and Fortuna (Fig. 1) (*3*). It also triggered numerous landslides and rock falls and caused widespread liquifaction in local river valleys. Analysis of 1296 surveys in the north coast area indicate that the Modified Mercalli intensity peaked at IX in the Petrolia region and decreased in approximately a radial pattern around the epicenter (Fig. 1). Both of the two large aftershocks produced peak intensities of VIII, although the pattern was somewhat different from the main shock.

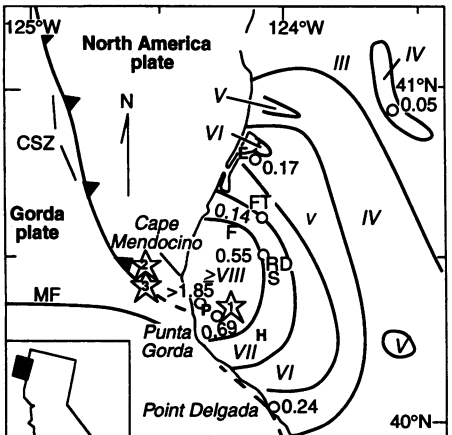

Fig. 1. Simplified tectonic map in the vicinity of the Cape Mendocino earthquake sequence. Stars, epicenters of three largest earthquakes; contours, Modified Mercalli intensities (values, Roman numerals) of main shock; open circles, strong motion instrument sites (*22*) (adjacent numbers give peak horizontal accelerations in *g*). Abbreviations: FT, Fortuna; F, Ferndale; RD, Rio Dell; S, Scotia; P, Petrolia; H, Honeydew; MF, Mendocino fault; CSZ, seaward edge of Cascadia subduction zone; and SAF, San Andreas fault.

Tectonic Setting

The Cape Mendocino earthquakes are a response to ongoing plate motions between the Gorda, North America, and Pacific plates at the Mendocino Triple Junction. The Gorda plate is converging on the North America plate at about 2.5 to 3 cm/year in the direction N50°E to N55°E (*4*). The seaward edge of Gorda plate subduction is marked by an abrupt change in sea-floor topography and by the western limit of the accretionary prism imaged in seismic reflection profiles (*5*). Active folds and thrust faults in Franciscan Complex and Cenozoic rocks and sediments of the overriding North America plate are parallel to the seaward edge of the Cascadia subduction zone (*6*).

Rigid plate theory predicts oblique convergence of the Gorda plate with the Pacific plate at 5 cm/year in the direction N115°E (*4*). Translational motion occurs along the east-west–trending, vertical, right-lateral Mendocino transform fault, whereas the convergence results in internal deformation of the Gorda plate. The attendant Gorda plate seismicity recorded in the 17 years before the Cape Mendocino sequence (*7, 8*) (Fig. 2) has been concentrated in two parallel zones with a combined thickness of approximately 15 km. In the region of the Cape Mendocino earthquake, most seismic-

D. Oppenheimer, J. Eaton, A. Jayko, M. Lisowski, G. Marshall, M. Murray, R. Simpson, and R. Stein are with the U.S. Geological Survey, Menlo Park, CA 94025. G. Beroza and M. Magee are in the Geophysics Department, Stanford University, Stanford, CA 94305. G. Carver, L. Dengler, and R. McPherson are in the Department of Geology, Humboldt State University, Arcata, CA 95521. L. Gee and B. Romanowicz are at the University of California, Seismographic Station, ESB 475, Berkeley, CA 94720. F. Gonzalez is with the National Oceanic and Atmospheric Administration's Pacific Marine Environmental Laboratory, Seattle, WA 98115. W. H. Li is with Geological Sciences, AJ-20, University of Washington, Seattle, WA 98195. K. Satake is in the Department of Geological Sciences, University of Michigan, Ann Arbor, MI 48109. P. Somerville is with Woodward-Clyde Consultants, Pasadena, CA 91101. D. Valentine is in the Department of Geological Sciences, University of California, Santa Barbara, CA 93106.

ity locates at depths greater than 17 km; the hypocenter zone dips about 6° eastward between 124.75° and 123.25°W, at which point the dip increases to about 25° (9). Most $M > 5$ earthquakes within the Gorda plate exhibit left-lateral motion on steep northeast-oriented faults (*7*, *10*) that relieve convergence between the Gorda and Pacific plates through slip on preexisting planes of weakness inherited at the Gorda Ridge (*11*).

The San Andreas fault marks the principal Pacific–North America plate boundary south of the Mendocino Triple Junction. Triangulation data and observations of ground cracks indicate the fault ruptured as far north as Point Delgada in 1906 (*12*), but its location farther north is uncertain. Some studies place it immediately offshore (*13*), but others suggest that it merges with onshore faults at the triple junction (*5*). Geometry requires that the Pacific plate is also in contact with the North America plate along the Mendocino fault above the subducting Gorda plate.

Until the Cape Mendocino earthquake, few earthquakes were recorded with focal mechanisms that indicated slip on the Cascadia subduction zone. However, comparisons of the age, spreading rates, physiography, and seismicity of the Juan de Fuca–Gorda plate system with other subducting plates suggest that it does not subduct aseismically but instead is locked and capable of generating major earthquakes (*14*). Paleoseismic evidence of large, late Holocene subduction earthquakes is present along the subduction zone in submerged and buried wetlands (*15*), raised marine terraces (*16*), and surface displacement on thrust faults that may be genetically related to large subduction events (*17*). Radiocarbon dating indicates that at least three episodes of seismicity of similar age are represented in the stratigraphy from central Washington to northern California in the last 2000 years; the last episode occurred at about 1700 A.D. (*17*).

Observations

Seismicity. The hypocenter of the 25 April 1992 main shock was located 4 km east of Petrolia at a depth of 10.6 km (Fig. 3). A focal mechanism determined by the inversion of teleseismic mantle Rayleigh waves and aftershock locations indicate nearly pure thrust motion on a N10°W-striking fault plane that dips 13° to the east-northeast (*18*) (Table 1). The location of the hypocenter at the southeast end of the aftershock zone suggests that the fault ruptured unilaterally to the west (*19*). Most aftershocks <12 km deep (Fig. 3, circles) occurred within 10 km of the coast in a region bounded on the east by the mainshock epicenter, on the south by the Mendocino fault, and on the north by a west-northwest trend of earthquakes. The location, depth, and orientation of the rupture plane are consistent with the absence of surface faulting onshore.

The two M_s 6.6 aftershocks were located 30 km west of the main shock at depths near 20 km, and their mechanisms indicate right-lateral, strike-slip motion on planes striking to the southeast (*20*) (Fig. 3 and Table 1). The slip plane of the first after-

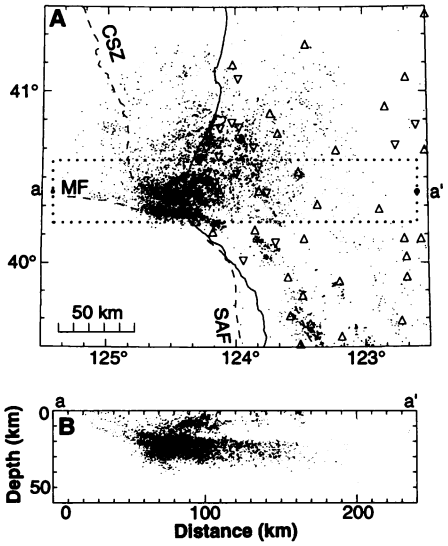

Fig. 2. Seismicity between August 1974 and time of main shock (*8*). (**A**) Locations of operating and discontinued seismic stations (upward and downward pointing triangles, respectively) at time of main shock. (**B**) Depths of earthquakes along cross section aa′. Depths west of longitude 124°40′W are unreliable. Note the gap in seismicity between main shock rupture plane at 10 km depth (Fig. 3B, aa′) and pre–main shock seismicity at depths greater than 17 km. The earthquakes at cross section distance 200 km occur at depths greater than 35 km and begin to image the region of the Gorda plate where the dip increases. Earthquakes as deep as 90 km occur near longitude 122°10′W (*9*).

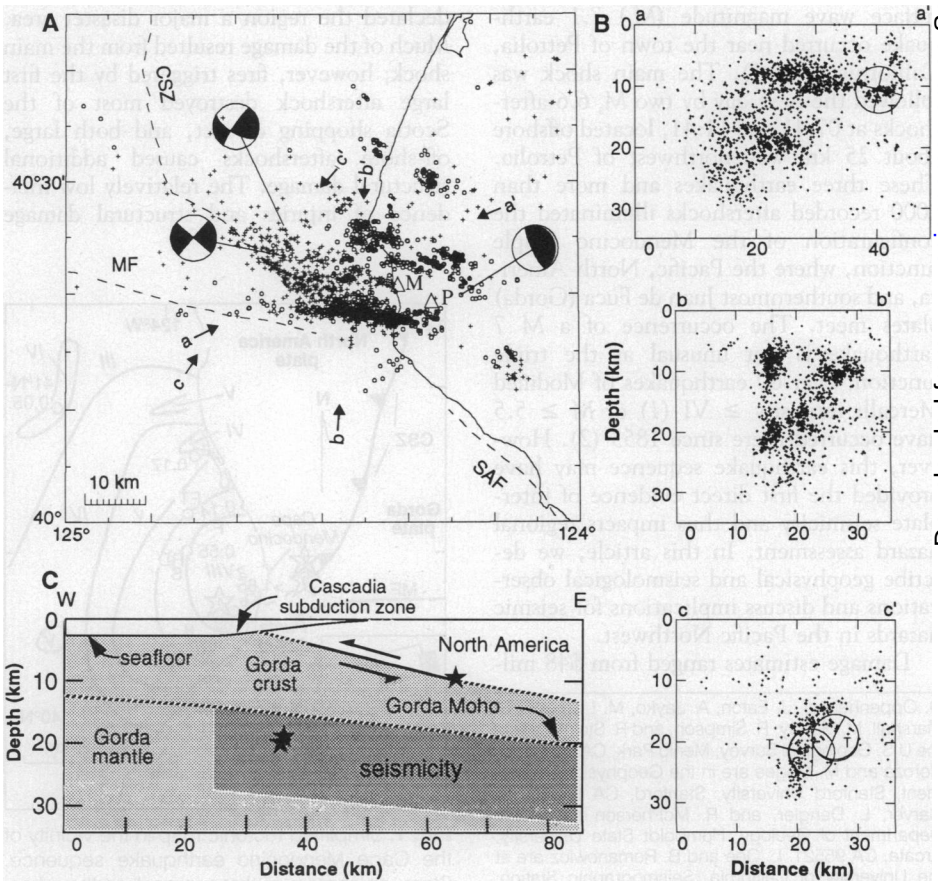

Fig. 3. (**A**) Focal mechanisms (lower hemisphere projections) of the main shock and two large aftershocks at their epicentral locations (compressional quadrants in black) and location of other aftershocks for 25 April 1992 to 30 September 1992 (circles for foci <12 km deep and plus symbols for deeper foci). (**B**) Depth of earthquakes on cross sections aa′ (perpendicular to main shock strike, width ± 20 km), bb′ (perpendicular to Mendocino fault, width ± 20 km), and cc′ (perpendicular to strike of M_s 6.6 aftershocks, width ± 9 km). Compressional quadrant marked by "T." (**C**) East-west cross section depicts location of main shock rupture plane (solid line), hypocenters (stars), and pre–main shock seismicity with respect to plausible interpretation of Gorda–North America plate geometry.

shock is unknown because of the paucity of aftershocks. However, the second aftershock was located within a trend of smaller aftershocks at depths of 14 to 30 km on a southeast-striking plane that dips about 80° to the southwest (Fig. 3B, cc'); this orientation is consistent with the focal mechanism. The depths and mechanisms of the two large aftershocks provide evidence that rupture took place on faults in the Gorda plate, distinct from the main shock fault.

Although no large shocks ruptured the Mendocino fault during this sequence, many aftershocks occurred on the eastward projection of the fault (Fig. 3). The aftershock activity was bounded on the south where the distribution of hypocenters is near vertical and extends to a depth of 25 km (Fig. 3B, bb'). If this marks the boundary between the Gorda and Pacific plates, then the lack of any aftershocks in the Pacific plate suggests that the main shock represented strain release between the Gorda and North America plates. The mapped location of the Mendocino fault in this region is uncertain (*5*), and this eastwest trend of seismicity may define the position of the Mendocino fault.

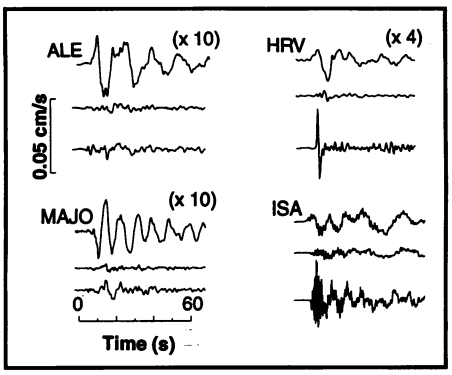

Fig. 4. Broad-band velocity records from four stations (ALE: epicentral distance Δ = 5185 km, azimuth = 9°; HRV: Δ = 4366 km, azimuth = 69°; MAJO: Δ = 8029 km, azimuth = 305°; ISA: Δ = 745 km, azimuth = 132°) for the main shock (top trace) and the first (middle) and second (lower) aftershocks. The amplitudes of the seismograms at ALE, HRV, and MAJO are increased relative to ISA for display. The large amplitudes of the second aftershock relative to the other two events in the along-strike azimuth (ISA) is attributable to rupture directivity.

Source properties. The mechanism and location of the two aftershocks were similar, but the second aftershock exhibited a strong variation of amplitude with azimuth (Fig. 4). The seismic moment of the second aftershock was approximately twice that of the first, but amplitudes of the P wave for this event were as much as 10 times as large near an azimuth of 130°. This variation is most easily attributable to enhancement of the amplitude in the direction of rupture, known as directivity (*21*). Directivity in P waves is surprising because it requires rupture velocities that are a large fraction of the P wave velocity. The high amplitudes and strong high-frequency content associated with the second aftershock may explain some of the differences in the intensity patterns for the main shock and two aftershocks. Although the second aftershock had 25% of the moment of the main shock, it has larger velocity amplitudes at stations to the southeast, such as ISA. The difference in both Modified Mercalli intensity and broad-band velocity records between the main shock and the second aftershock was probably enhanced by rupture propagation to the west during the main shock as inferred from the location of the hypocenter at the down-dip end of the rupture plane.

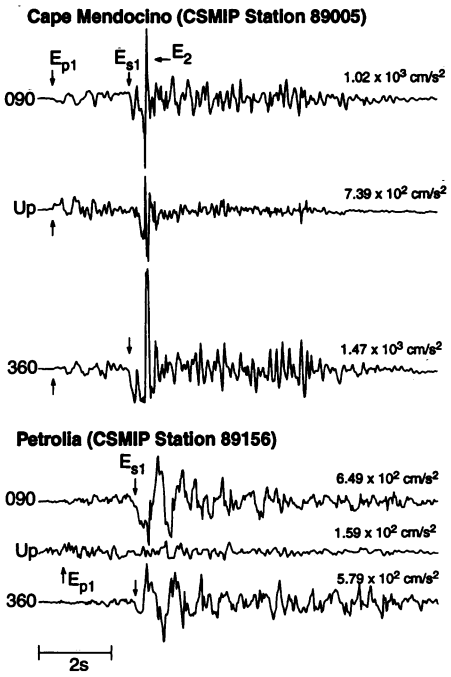

Fig. 5. Strong motion recordings and three components of the peak accelerations from stations of the California Strong Motion Instrumentation Program (CSMIP) at Cape Mendocino and Petrolia (*22*). Discernible first motion directions of the P and S waves for long-period event (E_{P1} and E_{S1}) are indicated, as is the large, high-frequency pulse at Cape Mendocino (E_2).

The strong ground motions of the main shock and two aftershocks were recorded on 14 instruments at epicentral distances of 5 to 130 km (Fig. 1), and the peak accelerations were some of the highest ever recorded (*22*). Recordings of the main shock at Petrolia and Cape Mendocino (Fig. 5) at epicentral distances of 5 and 10 km, respectively, have absolute time, facilitating the analysis of rupture evolution on the fault. Modeling of the large, long-period pulse that occurred 1 s after the main shock began (Fig. 5, E_{P1} and E_{S1}) with generalized ray theory indicates that this pulse originated from slip that occurred about 5 km up-dip from the hypocenter, beneath Petrolia. This result is consistent with the arrival times and polarities of the vertical P waves and horizontal S waves at both stations. In addition, the P wave first motions were upward and northwestward at Cape Mendocino. These motions indicate that the source was southeast of the station. This source location is consistent with the west-southwest direction of rupture determined from teleseismic surface waves (*19*), although that study inferred that the rupture initiated offshore. A large, high-frequency pulse (Fig. 5, E_2) followed the long-period pulse at Cape Mendocino and exceeded 1*g* on both horizontal components. This pulse was not discernible at the neighboring Petrolia station; thus, it cannot be explained simply by source effects but may represent motions that were generated or amplified locally near the Cape Mendocino station.

Table 1. Earthquake parameters.

	Origin time* (UTC)	Latitude* (North)	Longitude* (West)	Depth* (km)	Centroid depth† (km)	m_b‡	M_s‡	Moment† (dyn·cm)	Strike†	Dip†	Rake†
Main shock	25 April 18:06:05.16	40°19.94′	124°13.69′	10.6	20 to 25	6.3	7.1	4.45×10^{26}	349.7°	13.0°	105.6°
First aftershock	26 April 07:41:39.98	40°26.13′	124°34.43′	19.3	20 to 25	5.9	6.6	6.35×10^{25}	122.3°	75.9°	175.2°
Second aftershock	26 April 11:18:25.82	40°23.38′	124°34.30′	21.7	30 to 35	6.5	6.6	1.20×10^{26}	311.5°	89.6°	181.8°

*Hypocentral location determined from the local seismic network of the U.S. Geological Survey (*8*). †From surface-wave inversion (*18, 20*). ‡National Earthquake Information Center, Preliminary Determination of Epicenters.

Coseismic displacement. The elastic strain released by the main shock caused significant horizontal and vertical deformation in the epicentral region. The main shock elevated about 25 km of the coast from 3 km south of Punta Gorda to Cape Mendocino (Fig. 6). Many intertidal organisms inhabiting rocky reefs perished in the 3 weeks after the main shock. Maximum uplift was 140 ± 20 cm at Mussel Rock and 40 to 50 cm at the northernmost reef at Cape Mendocino (*23*). The lack of rocky intertidal environments farther north precluded the precise location of the northern limit of the uplift, but several near-shore rocks located about 7 km north of Cape Mendocino showed no evidence of uplift.

Coseismic horizontal and vertical site displacements in a regional geodetic network (Fig. 6) were determined from Global Positioning System (GPS) surveys in 1989, 1991, and 1 month after the main shock. The relative positions of most sites near the epicenter were measured shortly after the 17 August 1991 Honeydew earthquake [body wave magnitude (m_b) 6.0], which occurred 6 km south of the Cape Mendocino epicenter. The coseismic displacements were determined by comparison of the 1989 to 1992 observations, except in the vicinity of the Honeydew event where the 1991 survey was referenced. All displacements were corrected for secular strain accumulation estimated from Geodolite trilateration measurements made between 1981 and 1989. A site 13 km northeast of the epicenter had the largest measured coseismic displacement, moving 40 ± 2 cm to the west-southwest and subsiding 16 ± 8 cm.

Our preferred uniform-slip fault model (*24*), estimated from the coseismic site displacements and coastal uplift observations, indicates 2.7 m of nearly pure thrust motion occurred on a gently dipping fault plane. This model, chosen from a suite of acceptable models (*24*), is consistent with the main shock focal mechanism, the hypocenter location, and the distribution of aftershocks (Fig. 6 and Table 2). The range of geodetic moment inferred from the acceptable models is 2.5×10^{26} to 3.5×10^{26} dyn·cm, about 60% of the main shock seismic moment (Table 1). The model predicts a maximum uplift along the coast that is consistent with but somewhat less than the observed uplift. More complex models that use nonuniform slip to describe the rupture may improve these estimates of uplift and geodetic moment.

Table 2. Displacement model.

Parameter	Value
Width	16 km
Length	21.5 km
Depth to top edge	6.3 km
Latitude origin*	40°18.08′N
Longitude origin*	124°11.80′W
Depth at epicenter location	9.2 km
Moment†	2.79×10^{26} dyn·cm
Strike/dip/rake	350°/12.0°/94°
Slip	2.7 m

*Southeast corner of fault plane. †Assumes uniform rigidity of 3×10^{11} dyn/cm^2.

Tsunami. The main shock generated a small tsunami recorded by tide gauges along the California, southern Oregon, and Hawaii coastlines (Fig. 7). The largest tsunami amplitudes were recorded at Crescent City, California, where two well-defined packets of wave energy were recorded within the first 5 hours with maximum positive heights of 35 and 53 cm. Neither the precise arrival time nor the polarity of the first wave are clear because of the presence of background noise. However, the first packet of wave energy is consistent with the predicted travel time of 47 min for a wave ray path that traversed deep water. The second wave packet probably represents coastal trapped waves, or edge waves, having much slower velocities and amplitudes that rapidly decrease with distance offshore. Because the tsunami arrival nearly coincided with low tide at Crescent City, the wave did not cause any damage. The tsunami at Crescent City had an 8-hour duration; wave heights reached a maximum 3 to 4 hours after the first arrival. Tide gauges also recorded the initial arrival and subsequent edge waves at North Spit (Eureka, California) (20 min and 2.5 hours), Arena Cove (35 min and 3.5 hours), and Point Reyes (65 min and 3 hours).

Motion on the Plate Boundary

Interplate main shock. The main shock fault projects to the sea floor within 5 km of the seaward edge of the Cascadia subduction zone (*25*) (Fig. 3), suggesting that the main shock ruptured the Gorda–North America plate boundary. In contrast, the upper boundary of the pre–main shock seismicity, which is 7 km deeper than the main shock rupture plane (Figs. 2 and 3), projects to the surface about 85 km west of the Cascadia subduction zone and thus does not appear to define the plate boundary. The seismicity gap between the slip plane of the main shock and the pre–main shock seismicity is about the same thickness as the Gorda crust and overlying accretionary sediments, as determined from refraction experiments 10 km east of the seaward edge of the subduction zone (*26*). The gap may reflect a ductile subducted Gorda crust, and the inception of seismicity at a depth of 17 km may reflect brittle behavior of the Gorda upper mantle (*27*). Tabor and Smith (*28*) reached a similar conclusion from their observations of seismicity and velocity structure of the Juan de Fuca plate beneath the Olympic peninsula of Washington.

However, an inversion for the three-dimensional velocity structure of the region indicates that velocities typical of Gorda crust are evident at depths greater than 15 to 20 km (*29*). Moreover, modeling of

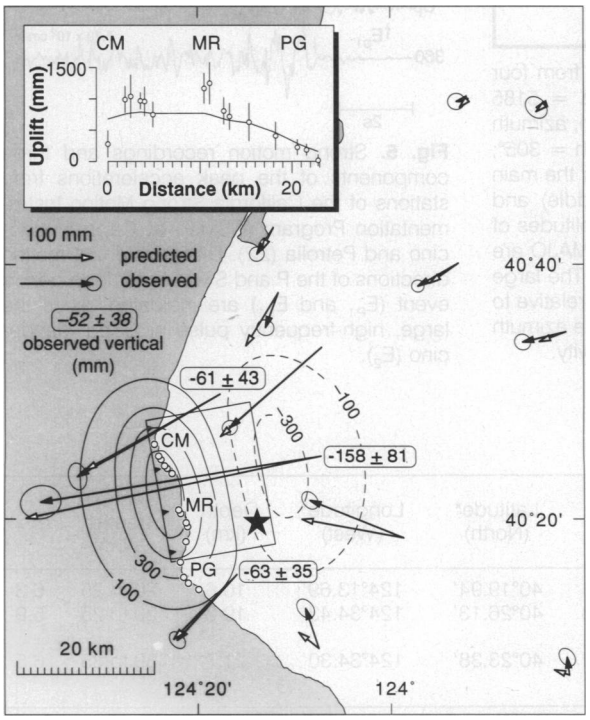

Fig. 6. Observed and predicted coseismic displacements for the Cape Mendocino main shock (epicenter located at star). The vectors are horizontal displacements relative to a site located at 41°9.20′N, 123°52.92′W. Observed displacements derived from GPS and Geodolite measurements; ellipses enclose regions of 95% confidence. Predicted displacements are from a model of uniform slip on the northeast-dipping rectangular fault plane, indicated by its surface projection. Rounded rectangles show vertical displacements measured by GPS that are greater than their standard deviations. Contours are elevation changes in millimeters predicted by the model. Abbreviations: CM, Cape Mendocino; MR, Mussel Rock; and PG, Punta Gorda. (**Inset**) Uplift measurements and their standard deviations from the die-off of marine organisms at coastal sites (open circles on map) and predicted uplift projected along N10°W.

thermal effects on the strength of the subducting oceanic lithosphere (*30*) suggests that the double seismic layers observed at depths of 20 and 30 km (Fig. 2) reflect, respectively, the brittle upper crust and upper mantle of the Gorda plate; the intervening, relatively aseismic region would correspond to the ductile lower crust. Consequently, these studies suggest that the Cape Mendocino main shock was an intraplate event in the North America plate.

Whether the main shock was an inter- or intra-plate event, the Cape Mendocino main shock clearly relieved strain resulting from the relative Gorda–North America plate motion. We note, however, that the main shock ruptured a region of the plate boundary that differs considerably from the boundary farther north, as indicated by the change in its orientation from north-northwest to northwest (*5*), the relatively narrow width of the plate, the likely presence of subducted sediments in the region of main shock rupture, and its younger age (*4*). Thus, this earthquake may not be typical of other Cascadia subduction zone earthquakes.

Intraplate aftershocks. The location, depth, and focal mechanisms of the two large aftershocks indicate that they ruptured the Gorda plate. The seismic data indicate that right-lateral slip occurred on a vertical, northwest-oriented fault plane for at least the second event. For most earlier Gorda shocks, rupture occurred as left-lateral slip on a northeast-oriented plane, perhaps because this orientation may allow reactivation of normal faults formed at the Gorda spreading ridge (*11*). From a consideration of stress release, either orientation reduces north-south compressional stress and down-dip tension in the Gorda plate, but rupture of the northwest-oriented plane may have been favored because of the static stress changes imposed by the main shock and, perhaps, the first aftershock.

To test this hypothesis, we modeled the changes in static stress (*31*) imposed by the main shock (Table 2) on three vertical fault planes: the east-west–oriented Mendocino fault, the possible N40°E-oriented slip plane of the first large aftershock, and the N50°W-oriented fault of the second large Gorda aftershock. Large regions of the northwest-oriented fault and the Mendocino fault received an increase in right-lateral shear stress greater than 3 bars and equally large increases in normal extension resulting from the main shock. Both the increase in right-lateral shear and the increased extension would bring both of these right-lateral faults closer to failure under a Coulomb failure criterion for nonzero coefficients of friction. About 90% of the aftershocks within 4 km of the Mendocino fault and the northwest Gorda fault occur where the modeling predicts the stress changes should load these faults toward failure for coefficients of friction ranging from 0.0 to 0.75. Thus, static stress changes may have helped trigger aftershocks along these two faults.

The model also indicates that static stress changes induced by the main shock are slightly more favorable for failure on a northeast-striking, left-lateral fault plane in the location of the first large aftershock, primarily because of a decrease in normal stress. In consideration of the present relative hypocentral locations of the two large aftershocks, slip on the northeast-oriented plane of the first aftershock would have added minor left-lateral shear to the northwest-oriented plane of the second aftershock but would have greatly decreased the normal stress on this plane. This scenario provides a simple mechanism in which the first aftershock helped trigger the second, similar to the scenario proposed for the Elmore Ranch–Superstition Hills pair of earthquakes (*32*).

Hazard implications. The Cape Mendocino earthquake sequence provided seismological evidence that the relative motion between the North America and Gorda plates results in significant thrust earthquakes. In addition to the large ground motions generated by such shocks, they can trigger equally hazardous aftershock sequences offshore in the Gorda plate and on the Gorda-Pacific plate boundary. This sequence illustrates how a shallow thrust event, such as the one of moment magnitude (M_w) 8.5 that is forecast for the entire Cascadia subduction zone (*14*), could generate a tsunami of greater amplitude than the Cape Mendocino main shock. Not only would this tsunami inundate communities along much of the Pacific Northwest coast within minutes of the main shock, but it could persist for 8 hours at some locales. The 25 April 1992 main shock ruptured only a small part of the plate boundary and apparently did not trigger slip on any of the Holocene shallow thrust faults observed onshore in the triple junction region (*17*). Thus, given the high level of historical seismicity and the emerging picture of many active faults, the region is likely to continue experiencing significant seismicity.

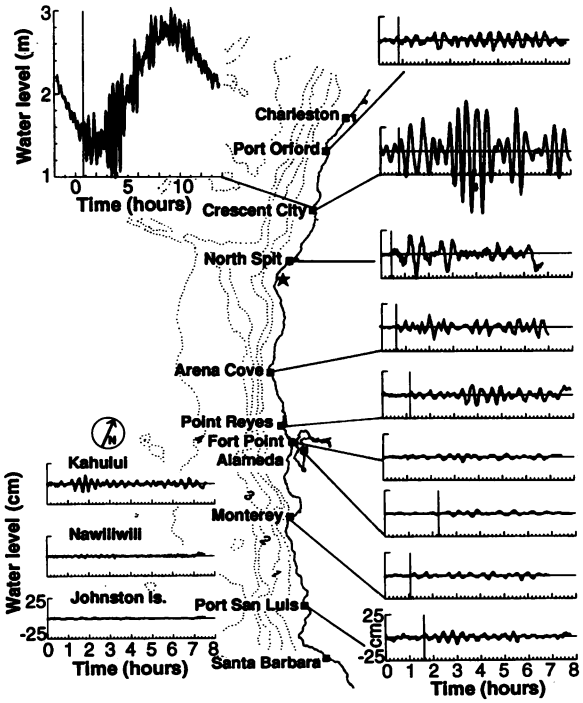

Fig. 7. Tsunami measurements at tide gauge stations along the coasts of California, Oregon, Hawaii, and Johnston Island. Tidal signal has been removed from all data except for Crescent City, California (inset) (note change of scale). Time of main shock is 0 hours. The vertical line marks the expected tsunami arrival time. Contour lines (dotted) represent ocean depth in kilometers, except for the single, unlabeled 500-m bathymetric contour line nearest the coast.

REFERENCES AND NOTES

1. H. O. Wood and F. Neumann, *Bull. Seismol. Soc. Am.* **21**, 277 (1931).
2. L. Dengler, G. Carver, R. McPherson, *Calif. Geol.* **45**, 40 (1992).
3. California Office of Emergency Services Situation Report, 4 May 1992; American Red Cross Disaster Update, 8 May 1992.
4. R. Riddihough, *J. Geophys. Res.* **89**, 6980 (1984); C. Nishimura, D. S. Wilson, R. N. Hey, *ibid.*, p. 10283; D. S. Wilson, *ibid.*, in press.
5. S. H. Clarke, Jr., *Am. Assoc. Pet. Geol. Bull.* **76**, 199 (1992).
6. H. M. Kelsey and G. A. Carver, *J. Geophys. Res.* **93**, 4797 (1988).
7. R. C. McPherson, thesis, Humboldt State University (1989).
8. Earthquakes for the period August 1974 to December 1984 were recorded by the Tera Corporation. Since 1983, the seismicity has been recorded by local networks operated by the U.S. Geological Survey and the University of California at Berkeley. All earthquake locations are based on a one-dimensional velocity model with station corrections developed from a joint hypocenter-velocity inversion of travel-time data and located with Hypoinverse [F. W. Klein, *U.S. Geol. Surv. Open File Rep. 89-314* (1989)]. Calibration explosions at Punta Gorda and Cape Mendocino were located to the northwest, 1.5 and 2.7 km, respec-

tively, at the surface. Locations of the offshore earthquakes are not as accurate as those onshore because of the network geometry.
9. R. S. Cockerham, *Bull. Seismol. Soc. Am.* **74**, 569 (1984); S. R. Walter, *ibid.* **76**, 583 (1986).
10. T. V. McEvilly, *Nature* **220**, 901 (1968); J. P. Eaton, *Eos* **62**, 959 (1981); T. J. Lay, J. W. Given, H. Kanamori, *Bull. Seism. Soc. Am.* **72**, 439 (1982).
11. D. S. Wilson, *J. Geophys. Res.* **94**, 3065 (1989).
12. A. C. Lawson, *Carnegie Inst. Washington Publ.* **87**, 54 (1908); W. Thatcher and M. Lisowski, *Eos* **68**, 1507 (1987).
13. J. R. Curray and R. D. Nason, *Geol. Soc. Am. Bull.* **78**, 413 (1967); L. Seeber, M. Barazangi, A. Nowroozi, *Bull. Seismol. Soc. Am.* **60**, 1669 (1970).
14. T. H. Heaton and H. Kanamori, *Bull. Seismol. Soc. Am.* **74**, 993 (1984); T. H. Heaton and S. H. Hartzell, *ibid.* **76**, 675 (1986).
15. B. F. Atwater, *Science* **236**, 942 (1987); M. E. Darienz and C. D. Peterson, *Tectonics* **9**, 1 (1990); A. R. Nelson, *Quat. Res.* **38**, 74 (1992); G. S. Vick, thesis, Humboldt State University (1989); D. W. Valentine, thesis, Humboldt State University (1992).
16. D. Merritts and W. B. Bull, *Geology* **17**, 1020 (1989).
17. S. H. Clarke, Jr., and G. A. Carver, *Science* **255**, 188 (1992).
18. We inverted for the main shock source parameters using the formalism of B. Romanowicz and T. Monfret [*Ann. Geophys.* **4**, 271 (1986)] and the spherical-Earth model PREM [A. M. Dziewonski and D. L. Anderson, *Phys. Earth Planet. Inter.* **25**, 297 (1981)] to correct for propagation effects. Rayleigh waves with periods between 140 and 320 s from a global distribution of stations were sampled at 10 frequencies.
19. An analysis of broad-band surface waves indicates that the main shock ruptured to the southwest (azimuth = 230°) with the largest moment release beginning 5 km from and extending to 20 km offshore [C. J. Ammon, A. A. Velasco, T. Lay, *Geophys. Res. Lett.* **20**, 97 (1993)].
20. For the aftershocks, we computed path-dependent amplitude and phase corrections based on analysis of the main shock. The approach of path-dependent corrections is advantageous for use of data at regional distances as well as shorter periods [M. Pasyanos and B. Romanowicz, *Eos* **73**, 372 (1992)].
21. H. Benioff, *Calif. Div. Mines Geol. Bull.* **171**, 199 (1955); A. Ben Menahem, *Bull. Seismol. Soc. Am.* **51**, 401 (1961).
22. A. Shakal *et al.*, *Calif. Div. Mines Geol. Rep. OSMS 92-05* (1992).
23. Where colonies of organisms were completely killed, the vertical range of the organisms represents a minimum measure of the uplift. On some reefs, only the upper parts of some colonies of plants and sessile animals, such as mussels, died. The vertical extent of mortality in these colonies provided the best basis for estimates of the amount of uplift. The mean and standard deviation of the vertical extent of mortality for each colony (Fig. 6, inset) is estimated from multiple measurements made by a laser total station with an instrument precision of 1 mm.
24. We assumed that slip is uniform on a rectangular, planar fault embedded in an elastic half space. We performed a Monte Carlo search of the parameters describing the geometry of the fault plane and, for each geometry, used the horizontal and vertical GPS and coastal-uplift data to estimate the magnitude and rake of the slip vector. The scatter of the residuals for the best fitting models, including our preferred model (Table 2), is 2.2 times the a priori observational errors. An F-ratio test indicates other models with residual scatter less than 2.6 times the a priori errors do not differ significantly from the best fitting models at the 95% confidence level.
25. In the projections, we assumed that faults are planar, the ocean depth is 2.3 km at the seaward edge of the Cascadia subduction zone at the latitude 40°27′N, and the mean elevation of the seismic network is 0.9 km. Main-shock parameters are from Table 1. We assumed the upper boundary of the background Gorda seismicity dips 6° east at a depth of 17.5 km at the coordinates of the main shock hypocenter.
26. G. G. Shor, P. Dehlinger, H. K. Kirk, W. S. French, *J. Geophys. Res.* **73**, 2175 (1968); S. W. Smith, J. S. Knapp, R. C. McPherson, *ibid.* **98**, 8153 (1993).
27. W. P. Chen and P. Molnar, *ibid.* **88**, 4183 (1983); P. Molnar and P. England, *ibid.* **95**, 4833 (1990).
28. J. J. Tabor and S. W. Smith, *Bull. Seismol. Soc. Am.* **75**, 237 (1985).
29. D. Verdonck and G. Zandt, *Lawrence Livermore Natl. Lab. Rep. UCRL-JC-111629* (1992).
30. K. Wang and G. Rogers, *Eos* **73**, 504 (1992).
31. We estimated static stress changes caused by the main shock using a rectangular dislocation surface (Table 2) in an elastic half-space [Y. Okada, *Bull. Seismol. Soc. Am.* **82**, 1018 (1992)] to stimulate the earthquake rupture. The results of the model are insensitive to small variations in the assumed fault geometries or slip distributions, although the maximum values and spatial details of the stress fields are.
32. K. Hudnut *et al.*, *Bull. Seismol. Soc. Am.* **79**, 282 (1989).
33. We thank B. Ellsworth, C. Weaver, D. Wilson, and D. Merritts for reviews of the manuscript. The measurement of coastal uplift was supported by a grant from the Pacific Gas and Electric Company.

RESEARCH ARTICLE

NMR Structure of a Specific DNA Complex of Zn-Containing DNA Binding Domain of GATA-1

James G. Omichinski, G. Marius Clore,* Olivier Schaad, Gary Felsenfeld, Cecelia Trainor, Ettore Appella, Stephen J. Stahl, Angela M. Gronenborn*

The three-dimensional solution structure of a complex between the DNA binding domain of the chicken erythroid transcription factor GATA-1 and its cognate DNA site has been determined with multidimensional heteronuclear magnetic resonance spectroscopy. The DNA binding domain consists of a core which contains a zinc coordinated by four cysteines and a carboxyl-terminal tail. The core is composed of two irregular antiparallel β sheets and an α helix, followed by a long loop that leads into the carboxyl-terminal tail. The amino-terminal part of the core, including the helix, is similar in structure, although not in sequence, to the amino-terminal zinc module of the glucocorticoid receptor DNA binding domain. In the other regions, the structures of these two DNA binding domains are entirely different. The DNA target site in contact with the protein spans eight base pairs. The helix and the loop connecting the two antiparallel β sheets interact with the major groove of the DNA. The carboxyl-terminal tail, which is an essential determinant of specific binding, wraps around into the minor groove. The complex resembles a hand holding a rope with the palm and fingers representing the protein core and the thumb, the carboxyl-terminal tail. The specific interactions between GATA-1 and DNA in the major groove are mainly hydrophobic in nature, which accounts for the preponderance of thymines in the target site. A large number of interactions are observed with the phosphate backbone.

The erythroid-specific transcription factor GATA-1 is responsible for the regulation of transcription of erythroid-expressed genes and is an essential component required for the generation of the erythroid lineage (*1*). GATA-1 binds specifically as a monomer to the asymmetric consensus target sequence (T/A)GATA(A/G) found in the cis-regulatory elements of all globin genes and most other erythroid-specific genes that have been examined (*2*). GATA-1 was the first member of a family of proteins, which now includes regulatory proteins expressed in other cell lineages, characterized by their recognition of the GATA DNA sequence and by the presence of two metal binding regions of the form Cys-X-X-Cys-$(X)_{17}$-Cys-X-X-Cys separated by 29 residues (*2*, *3*). Mutation and deletion studies on

J. G. Omichinski, G. M. Clore, O. Schaad, and A. M. Gronenborn are in the Laboratory of Chemical Physics, Building 5, National Institute of Diabetes and Digestive and Kidney Diseases, National Institutes of Health, Bethesda, MD 20892. G. Felsenfeld and C. Trainor are in the Laboratory of Molecular Biology, Building 5, National Institute of Diabetes and Digestive and Kidney Diseases, National Institutes of Health, Bethesda, MD 20892. E. Appella is in the Laboratory of Cell Biology, Building 37, National Cancer Institute, National Institutes of Health, Bethesda, MD 20892. S. J. Stahl is in the Protein Expression Laboratory, Building 6B, Office of the Director, National Institutes of Health, Bethesda, MD 20892.

*To whom correspondence should be addressed.